Animal Nutrition 10 (2022) 111–123

Contents lists available at ScienceDirect

Animal Nutrition

journal homepage: http://www.keaipublishing.com/en/journals/aninu/

Original Research Article

Gut microbiota-derived metabolites contribute negatively to hindgut barrier function development at the early weaning goat model

Ke Zhang [a, 1], Yangbin Xu [a, 1], Yuxin Yang [a, 1], Mengmeng Guo [b], Ting Zhang [a], Bo Zong [a], Shuhong Huang [a], Langda Suo [c], Baohua Ma [b], Xiaolong Wang [a], Yujiang Wu [c], Daniel Brugger [d, *], Yulin Chen [a, *]

[a] Key Laboratory of Animal Genetics, Breeding and Reproduction of Shaanxi Province, College of Animal Science and Technology, Northwest A&F University, Yangling, 712100, China
[b] College of Veterinary Medicine, Northwest A&F University, Yangling, 712100, China
[c] Institute of Animal Sciences, Tibet Academy of Agricultural and Animal Husbandry Sciences, Lhasa, 850009, China
[d] Institute of Animal Nutrition and Dietetics, Vetsuisse-Faculty, University of Zurich, 8057, Zurich, Switzerland

ARTICLE INFO

Article history:
Received 24 August 2021
Received in revised form
27 December 2021
Accepted 11 April 2022
Available online 21 April 2022

Keywords:
Hindgut microbiome
Ruminant
Dysbiosis
Inflammation
Colon

ABSTRACT

Early weaning induces intestinal injury, leading to a series of long-term symptoms such as inflammation, malabsorption and diarrhea. In this study, we hypothesized that microbes and their metabolites modulate the host's inflammatory response to early weaning stress in a goat model. A total of 18 female Tibetan goat kids ($n = 9$) were weaned from their mothers at 28 d (D28) and 60 d (D60) postpartum. D60 and D28 groups were fed the same solid diet ad libitum from weaning to 75 d of age. The colonic epithelium was subject to RNA-sequencing, the caecal digesta metabolomics were assessed by liquid chromatography–tandem mass spectrometry (LC-MS/MS), and the caecal microbiota composition was analysed by 16S ribosomal RNA gene sequencing. We found that early weaning substantially increased the colonic pro-apoptotic gene expression of B-cell lymphoma associated X (*Bax*), caspase-9, and caspase-3, and decreased the expression of zonula occludens-1 (*ZO-1*) and claudin-1 ($P < 0.01$). In addition, a significant *Bacteroides acidifaciens* enrichment was observed in the hindgut of early-weaned goats ($P < 0.01$), which negatively correlated with lysophosphatidylcholine products. Similarly, the chemokine signaling, *IL-17* signaling, and peroxisome proliferators-activated receptor (*PPAR*) signaling pathways were upregulated in the colonic mucosa of the early-weaned goats. By applying caecal microbiota transplantation from goats to defaunated C57/6J mice, we confirmed that caecal microbiota of D28 goat kids increased the relative abundance of *B. acidifaciens* and significantly up-regulated the genes of *Bax*, G protein–coupled receptor (*GPR*) *109A*, *GPR 43*, fatty acid binding protein 6, nuclear receptor subfamily 1 group H member 3, angiotensin converting enzyme 2, and *IL-6* expression ($P < 0.05$), and decreased *ZO-1*, and claudin-1 protein expression in the mice jejunum and colon ($P < 0.001$). These results proposed that the hindgut microbiota and metabolites mediate the barrier function weakening during early weaning, and the relative abundance of *B. acidifaciens* was negatively correlated with the hindgut barrier gene expression. This study demonstrates how weaning stress can affect key host–microbe interaction regulators in the hindgut, in a lysophosphatidylcholine dependent and independent manner. Furthermore, based on our mice data, these results are transferable to other mammal species.

* Corresponding authors.
E-mail addresses: dbrugger@nutrivet.uzh.ch (D. Brugger), chenyulin@nwafu.edu.cn (Y. Chen).
[1] These authors contributed equally to this work.
Peer review under responsibility of Chinese Association of Animal Science and Veterinary Medicine.

Production and Hosting by Elsevier on behalf of KeAi

1. Introduction

Intensive livestock production systems include an early-weaning method for the benefit of productivity and reproduction (Belanche et al., 2019). Twenty-eight days postpartum appears to be the most common weaning age for small ruminants, but the optimal weaning age is controversially debated (Li et al., 2018;

https://doi.org/10.1016/j.aninu.2022.04.004

Wang et al., 2019). We previously investigated microbiota in the rumen of pre-weaned goats and found that the bacterial colonization in the rumen is already stabilized at 28 d postpartum (Lei et al., 2018; Zhang et al., 2019); whereas, the intestinal microbiota seem to reach their steady state earliest at 42 d of age (Li et al., 2019a). Interestingly, rumen development also affects the microbial composition in the hindgut of growing ruminants during the pre-weaning period. Shifts in the relative abundance of short-chain fatty acid (SCFA)-producing bacteria indicated that the hindgut microbiota play an important role for the host's dietary energy utilization in monogastric and ruminant animals (Song et al., 2017). The hindgut microbiota further affected gut immunity, inflammation, and intestinal barrier function by modulating the host–microbe interactions (Lyte et al., 2018). Further studies have shown that disturbed phylogenetic and functional adaption of gut microbiota are common consequences of weaning stress (Kosior-Korzecka et al., 2019) and are promoting the incidence of post-weaning diarrhea (Yu et al., 2020). In contrast, other studies challenged the persistent effects of early weaning in animals (Li et al., 2018; McCoard et al., 2020; Moeser et al., 2017). Therefore, the effects of early weaning on the host–microbe interactions in the ruminants' hindguts and its consequences for animal health warrant further research.

The intestinal epithelium directly interacts with biotic stressors and modulates and executes the immune response to them. To do so, the intestinal epithelial cells express pattern recognition receptors (*PRR*), such as toll-like receptors (*TLR*) and nucleotide binding oligomerization domain like receptors (*NLR*), which detect microbial pathogens and subsequently mediate the associated immune response (Fukata and Arditi, 2013; Medzhitov and Janeway, 2002). The intestinal epithelia respond to biotic stress by involving the Ig A transfer into the gut lumen via the polymeric immunoglobulin receptor and secreting further anti-microbial peptides, cytokines, and chemokines (Artis, 2008).

Recently, attention has been given to butyrate and its benefits on cellular energy metabolism and intestinal homeostasis (Guilloteau et al., 2010). Butyrate acts as a histone deacetylase inhibitor (HDACi), affecting several specific G protein-coupled receptors to regulate the biological response of the host's gastrointestinal health (De Clercq et al., 2016). It also plays an essential role in regulating immune and inflammatory response and intestinal barrier function (Liu et al., 2018). It has been further shown that butyric acid provides about 70% of the energy for normal intestinal epithelial cells, promotes cell growth and proliferation at low concentrations, acts as HDACi to inhibit the proliferation of intestinal epithelial cells, and promotes their apoptosis at high concentrations (more than 5 mmol/L) (Andriamihaja et al., 2009; Gonalves and Martel, 2013). Furthermore, the utilization of butyrate as an energy substrate by intestinal epithelial cells occurs by β-oxidation and the associated significant oxygen consumption renders the conditions at the intestinal mucosa and in the gut lumen hypoxic, which is beneficial for commensal bacteria and suboptimal for facultative anaerobic pathogens, e.g. *Escherichia coli* and *Salmonella* spp. (Byndloss et al., 2017; Litvak et al., 2017). On the contrary, reduced microbial butyrate production in the hindgut forces the intestinal epithelial cells towards anaerobic glycolysis thereby causing higher oxygen levels in the mucus, which is detrimental for gut health due to better growth conditions for said pathogens (Litvak et al., 2017; Rivera-Chávez et al., 2016). In tumor cells, butyric acid accumulates in the nucleus as HDACi to regulate gene expression, thereby inhibiting their proliferation, and inducing apoptosis (Gonalves and Martel, 2013; Lazarova and Bordonaro, 2016). There is still uncertainty regarding the negative interaction between gut microbiota and their metabolites resulting in intestinal injury and inflammation, as witnessed especially in the hindgut of early weaned animals including ruminants.

In this study, we hypothesized that hindgut microbiota dysbiosis induced by early weaning plays a significant role in goat kids, and intestinal microbiota transplantation (IMT) can prevent inflammation and improve mucosal barrier function by restoring the gut microbiota in defaunated C57/6J mice. Therefore, we used 16S rRNA gene sequencing, metabolomics, host transcriptomic profiling, and IMT to investigate the early weaning effects on hindgut microbiota composition, metabolic adaption, and the physiological response of the epithelium, with special emphasis on the epithelial barrier function. We aimed to provide new insights into the underlying mechanisms affecting the hindgut metabolome and gut physiology.

2. Materials and methods

The experiment was approved by the Institutional Animal Care and Use Committee of the Northwest A&F University under permit number 2018XZ0716003.

2.1. Animals, diets, and experimental design

This study was conducted at the experimental facilities of the Animal Husbandry and Veterinary Institute of Tibet Autonomous Region. A total of 18 female Tibetan goat kids ($n = 9$) were weaned from their mothers at 28 and 60 d postpartum, grouped by D28 and D60, respectively. In both D28 and D60 groups, goat kids were fed a starter diet after weaning. The goat kids were housed with their mothers prior to weaning, and then were separated from their mothers and abruptly weaned at the specified time points. D60 and D28 groups were fed the same starter diet ad libitum until age 75 d. Before weaning, breast milk was the only source of nutrition for all goat kids. Weaned goat kids were housed in pens (6 m × 9 m; $n = 3$ kids per pen) in the same environmentally controlled room. All goat kids had ad libitum access to the same diet and water. The diets of goat kids were formulated meeting or exceeding the current feeding recommendations (COUNCIL and Nutrient, 1981) (Appendix Table 1). The dietary and nutrient composition of maternal during the study is provided in Appendix Table 2. The body weight was analyzed at 0, 28, 35, 42, 56, 63, 70 and 75 d after birth of goats, respectively. The starter diet intake of D28 group was analyzed at 35, 42, 56, 63, 70 and 75 d after birth of goats, and the average weekly intake was 155.56, 167.88, 183.21, 188.97, 199.33, and 200.38 g/d based dry matter each goat kid, respectively. The starter diet intake of D60 group was analyzed at 63, 70 and 75 d after birth of goats, and the average weekly intake was 190.17, 211.35, and 197.93 g/d based dry matter each goat kids, respectively. At 75 d, 5 female goat kids were randomly selected from each group and 10 in total were sacrificed when they attained 75 d of age after being fasted for 12 h. They were euthanized via injection using thiopental (0.125 mg/kg of body weight) and potassium chloride (5 to 10 mL) (Fig. 1A). We then snap-froze the homogenized digesta from the cecum in liquid nitrogen and stored at −80 °C for subsequent DNA analysis. The colon epithelial tissue was excised from the mucosa layers by glass slide, and then immediately washed in ice-cold phosphate-buffered saline (PBS) until the PBS was clear, and then directly transferred into liquid nitrogen until tissue RNA extraction.

Five goat kids (mix pool of cecum content of each group) from D28 and D60 groups were used for cecum digesta transplantation. The caecal content (200 mg) from the donors was suspended in sterile 0.9% saline (2 mL) and centrifuged at 800 ×

g at 4 °C for 5 min to obtain the bacterial suspension. Twenty-four adult female C57/6J mice were divided into 4 groups: Con, a control group (without any treatment); Ab, an antibiotic group, which received sterile saline via gavage after antibiotic treatment stopped; D28_IMT, a group that was transplanted with group D28 cecum microbiota after antibiotic treatment stopped; and D60_IMT, a group that was transplanted with D60 cecum microbiota after antibiotic treatment stopped. Ab, D28_IMT, and D60_IMT groups were first treated with fresh composite antibiotics (containing 1 g/L ampicillin, 1 g/L streptomycin, 1 g/L gentamicin, and 0.5 g/L vancomycin; MACKLIN, China) using water for 14 d (Ren et al., 2018). Each recipient mouse received 200 μL of the supernatant by oral gavage once a day continuously for 7 d. To improve the cecum microbial survival rates during the cryopreservation, cecum content samples were diluted with sterile saline, homogenized and filtered. Subsequently, the resulting suspension was added to glycerol to get a final concentration of 10%. Finally, the cecum suspensions are labeled accurately, and stored in liquid nitrogen as soon as possible to ensure cecum microbial survival. When there is the need for IMT, the frozen cecum suspension was thawed at 37 °C (water bath). Upon frozen fecal suspension thawing, sterile saline solution can be added to obtain a required concentration (CFU = 1×10^9) and the infusion of cecum suspension should be implemented as soon as possible at 37 °C. All cecum material preparation processes were carried out at an anaerobic incubator (LAI-3T, Longyue, China). After transplantation, they were housed individually at room temperature (23 ± 1 °C) and light control (16L:8D) with free access to feed (Appendix Table 1) and drinking water. Body mass was measured every day. Mice were sacrificed after 7 d of IMT (at 10:00), and the caecal contents, jejunal and colon tissue were collected after the mice were euthanized via CO_2 inhalation then cervical dislocation. All samples were stored at −80 °C for subsequent DNA analysis. Jejunum tissue was stored in 4% paraformaldehyde in a refrigerator at 4 °C.

2.2. Serum parameters

Jugular vein blood was collected from the goats 1 h before slaughtering, preserved in the vacuum tube containing coagulant, kept at 4 °C for 3 h, then centrifuged at 1,789 × g at 4 °C for 10 min. The serum was used to determine IgA, IgG, IgM, urea-N, glucose (Glu), hydroxyl radical (.OH), hypoxia-inducible factor 1-beta (HIF-1β), cortisol (Cor), corticosterone (Cort), diamine oxidase (DAO), glutathione peroxidase (GSH-Px), superoxide dismutase (SOD), total protein (TP), albumin (ALB), globulin (GLB), total cholesterol (TC), triglycerides (TG), IL-1β, tumor necrosis factor-α (TNF-α), and IL-6.

2.3. 16S rRNA gene profiling

A total of 10 luminal samples from cecum were collected from the D28 and D60 groups. Total DNA was then extracted from the cecum lumen content using the E.Z.N.A. stool DNA Kit (Omega Bio-Tek, Norcross, GA, USA), according to the manufacturer's instructions. The Nanodrop 2000 UV-VI spectrophotometer (Thermo Scientific, Wilmington, USA) was used to determine the DNA concentration and purity. A 1% agarose gel electrophoresis was used to assess the quality of the extracted DNA. The primers 338F (5′-ACTCCTACGGGAGGCAG CAG-3′) and 806R (5′-GGACTACHVGGGTWTCTAAT-3′) on a thermocycler PCR system (Gene Amp 9700, ABI, USA) were used to amplify the V3–V4 region of the DNA (Lin et al., 2020). The paired-end sequencing (2 × 300 bp) on an Illumina MiSeq platform (Illumina, San Diego, USA) was conducted according to the standard Major Biobio-Pharm Technology Co. Ltd. (Shanghai, China) protocols on the pooled equimolar ratios of the purified amplicons.

2.4. Measurement of short-chain fatty acids

The Agilent 7820A gas chromatograph (Agilent Technologies, Santa Clara, USA) was used to measure the SCFA concentrations in content samples from the cecum (Li et al., 2014).

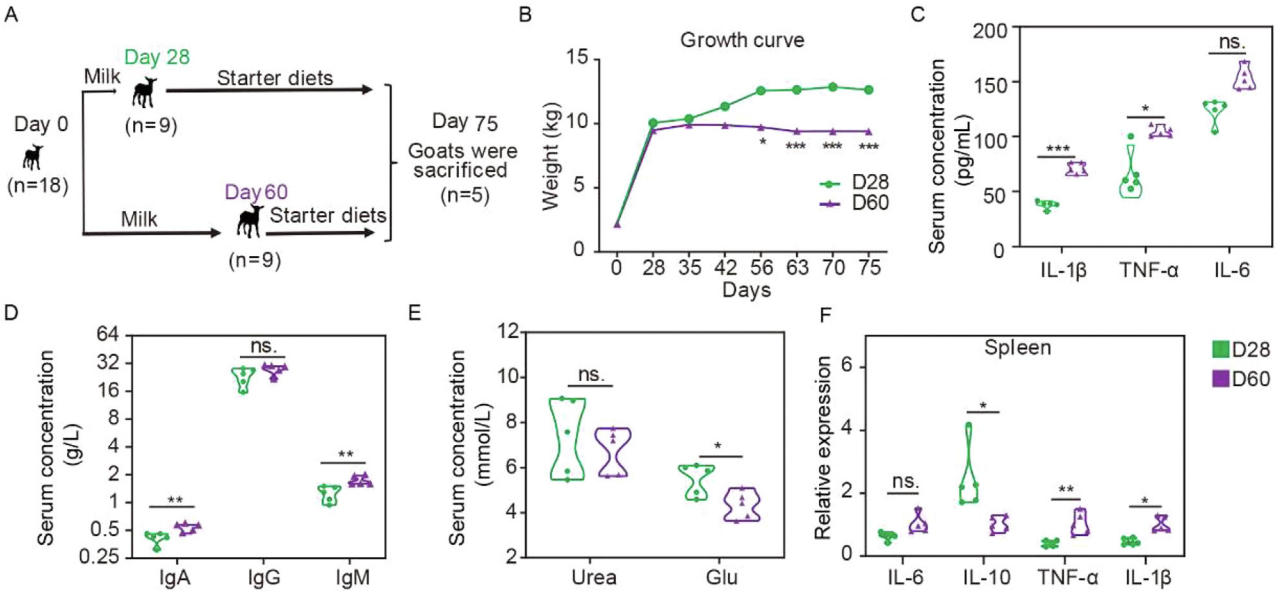

Fig. 1. Effects of early weaning in goats on the body weight and serum parameters. (A) The design paradigm. (B) Early weaning increases the body weight after 56 d ($n = 9$ individuals/group). (C) Serum inflammatory factor concentration ($n = 5$ individuals/group). (D) Serum urea-N, glucose concentrations ($n = 5$ individuals/group). (E) Serum IgA, IgG, and IgM concentrations ($n = 5$ individuals/group). (F) Gene expression of *IL-6*, *IL-10*, tumor necrosis factor-α (*TNF-α*), and *IL-1β* in goats' spleen ($n = 5$ individuals/group). D28 and D60 represent the goat kids were weaned from their mothers at 28 and 60 d. Data differences in goat subjects were assessed using the one-way ANOVA with Tukey's test. Not significantly different (ns.) $P > 0.05$, $^*P < 0.05$, $^{**}P < 0.01$, and $^{***}P < 0.001$.

2.5. RNA isolation and RNA-seq analyses

TRIzol Reagent was used according to the manufacturer's instructions (Invitrogen) to extract the total RNA from the goat colon epithelial tissue and the DNase I (TaKaRa) used to remove genomic DNA. The 2100 Bioanalyser (Agilent) and the Nanodrop 2000 UV-VI spectrophotometer (Thermo Scientific, Wilmington, USA) determined the RNA quality (RIN number: 7.10, 8.90, 8.80, 7.00, 7.90 in D28 group samples, respectively, 10.00, 9.80, 8.40, 8.60, 9.80 in D60 group samples, respectively). Five micrograms of total RNA was used to prepare the RNA-seq transcriptome library following the TruSeq RNA sample preparation Kit from Illumina (San Diego, CA). A Paired-end RNA-seq sequencing library was sequenced using the Illumina HiSeq 4000 (2 × 150 bp read length) after TBS380 quantification. The SeqPrep (https://github.com/jstjohn/SeqPrep) and Sickle (https://github.com/najoshi/sickle) with default parameters were used to trim and control the raw paired-end reads. Clean reads were then separately aligned to the *Capra hircus* (goat) reference genome (GenBank assembly accession: GCA 001704415.1) using orientation mode with TopHat (v2.1.1) (Trapnell et al., 2009) software.

2.6. Cecum content metabolite measurements using LC-MS/MS

A volume of 500 μL of ice-cold methanol-to-water (70%, vol:vol) solution was used to homogenize the total 50 mg cecum content of the goats. The sample was then vortexed for 3 min, sonicated for 10 min in an ice water bath, and vortexed for 1 min. The sample was then centrifuged at 16,099 × *g* at 4 °C for 10 min. The collected supernatant was subjected to LC-MS/MS analysis (UPLC, Shim-pack UFLC SHIMADZU CBM A system, https://www.shimadzu.com/; MS, QTRAP System, https://sciex.com/).

2.7. Quantitative PCR (qPCR) analysis

Total RNA extraction and cDNA synthesis were performed as previously described (Liu et al.; Wang et al., 2018). Briefly, Trizol reagent (Invitrogen, Carlsbad, CA, USA) was used to extract the total RNA based on the manufacturer's protocols. The concentration and quality of total RNA were determined with a NanoDrop ND2000 spectrophotometer (NanoDrop Technologies, Wilmington, USA). The absorbed optical density ratio (OD260/280) for RNA was selected to maintain a high RNA purity (1.85 to 2.05), and the RNA integrity was verified by 1.4% agarose-formaldehyde gel electrophoresis. qPCR was performed using CFX96 Real-Time PCR Detection System (Bio-Rad Laboratories, Hertfordshire, UK). Mice and goat primers for qPCR are shown in Appendix Table 3. In this study, Primer-BLAST (Ye et al., 2012) (https://www.ncbi.nlm.nih.gov/tools/primer-blast/) was used to design target-specific PCR primers, and Oligo 7 primer analysis software was used to assess the availability of primers. All the primers were sourced from ZhongKe Biotechnology (Shaanxi, China). The copy numbers of the 16S rRNA genes related to the *Bacteroides acidifaciens* and *Bacteroides uniformis* populations were enumerated via real-time PCR as previously described (Zhang et al., 2021), which was performed with the SYBR Premix Ex Taq II assay kit (TaKaRa Bio Inc., Shiga, Japan) using a CFX96 Real-Time PCR Detection System (Bio-Rad Laboratories, Hertfordshire, UK). The primers for *B. acidifaciens* were as follows: bacF (5′-GTATGGGATGGGGATGCGTT-3′) and bacR (5′- CTGCCTCCCGTAGAGTTTGG-3′) (Busbee et al., 2020), and the primers for *B. uniformis* were as follows: bacF (5′-TCACTCTTCGCGCCTT-3′) and bacR (5′-GTTCTCATGCACCGCTCA-3′). The reaction conditions were as follows: 95 °C for 30 s, followed by 40 cycles at 95 °C for 10 s and 60 °C for 30 s. The ΔΔCt method with *GAPDH* and *β-actin* were used as the reference genes to calculate the relative expression. Each goat's target gene expression was normalized to *GAPDH* expression, and that of mice was normalized to *β-actin* expression. The normalized data were presented in the treatment group's gene expressions the fold change compared to control. Standard and quantified samples were used in triplicate (Li et al., 2019a).

2.8. ZO-1 and claudin-1 measurement using immunohistochemistry

Immunohistochemistry was performed using the specific rabbit monoclonal antibody to analyze intestinal ZO-1 and claudin-1 expression distribution in mice. Claudin-1 antibody (13050-1-AP, Proteintech, USA) and ZO-1 antibody (21773-1-AP, Proteintech, USA) were used in the immunohistochemistry assay. Quantitative image analysis of the claudin-1 and ZO-1 immunoreactive cortical regions was performed on five fields using Image-Pro Plus 6.0 software as previously described (Liu et al., 2017).

2.9. Western blot

For total protein extraction, RIPA lysis buffer (P0013K, Beyotime, China) was utilized to lyse the tissues. Then, the lysate was centrifuged at 12,000 × *g*, 4 °C for 10 min to obtain the total protein. The protein concentrations were detected by the BCA Protein Assay Kit (ZJ102, EpiZyme, China) and Western blot was performed using sodium dodecyl sulfate polyacrylamide gel electrophoresis (SDS-PAGE) method. As described in our previous study (Li et al., 2019b). The transferred membranes were incubated at 4 °C overnight with the following primary antibodies: mouse anti-claudin-1 antibody (1:1,000, 13050-1-AP, Proteintech, USA), mouse anti-ZO-1 antibody (1:1,000, 21773-1-AP, Proteintech, USA) and β-tubulin (1:10,000, 10094-1-AP, Proteintech, USA). The blots were visualized using Bio-Rad ChemiDoc touch system (Bio-Rad, CA, USA), and the densities were analyzed by Image J software.

2.10. Statistical analyses

GraphPad Prism (V 8.3, GraphPad, USA) was used to generate violin plots. Data were presented as mean with standard error of the mean (SEM) or violin plots. One-way analysis of variance (ANOVA) with Tukey's multiple comparisons test was used via SPSS (V21, IBM, USA). The aligned unclassified or no rank operational taxonomic units (OTU) were used to construct a phylogenetic tree using the maximum likelihood in the IQ-TREE (version 1.6.8). We used OTU sequence alignment to the National Center for Biotechnology Information (NCBI) database to find the strains with the highest query cover, and download strains to construct phylogenetic tree (Bravo et al., 2018). The Shannon index were selected to calculate the alpha diversity of gut microbial composition at the OTU level, and Wilcoxon Rank–Sum test was used to analyze the significant differences of the alpha diversity index among different groups. Beta diversity indices (Bray–Curtis) were calculated in QIIME (V1.9.1) (Lawley and Tannock, 2017). Analysis of similarity (ANOSIM) of Bray–Curtis distances was performed to assess the statistical significance of differences in the bacterial community between different groups of samples. The differences in the relative abundance of bacterial taxa between groups were identified using the Kruskal–Wallis H test in the free online platform of Majorbio Cloud Platform (www.majorbio.com). The microbial components whose sequences were more abundant in the different groups were identified using linear discriminant analysis effect size (LEfSe). The non-parametric factorial Kruskal–Wallis (KW) sum-rank test followed by linear discriminant analysis (LDA) was performed for LEfSe to assess the effect

size of each differentially abundant taxon. Microbiota with substantially increased numbers was defined as having an LDA score (log 10) of more than 3.5. *P*-values of mice microbiota data were adjusted into false discovery rate (FDR) using the Benjamini-Hochberg method. $P < 0.05$ was considered statistically significant and *P* in the figures are denoted using asterisks (*$P < 0.05$; **$P < 0.01$; ***$P < 0.001$). Check online supplementary data: Supplemental method for additional information.

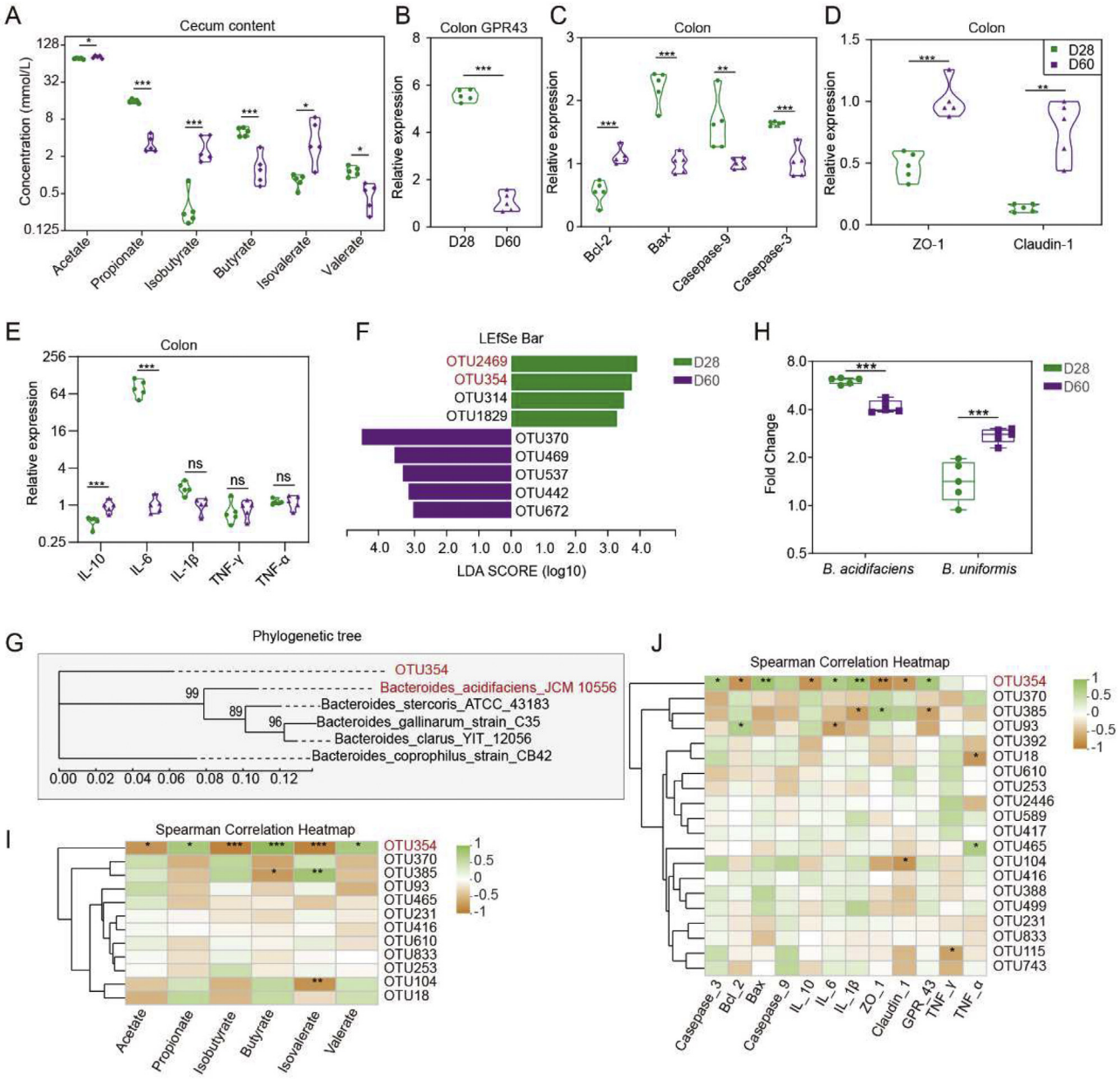

Fig. 2. Early weaning strategies alter hindgut microbiota composition and intestinal barrier function. (A) Fermentation parameters of the goats' cecum content. Differences in data were assessed by the one-way ANOVA with Tukey's test. (B) Gene expression of G protein–coupled receptor (*GPR*) *43* in the colon of goats. Differences in data were assessed by the one-way ANOVA with Tukey's test. (C) Apoptotic related gene expression in the colon of goats. Differences in data were assessed by the one-way ANOVA with Tukey's test. (D) Colonic barrier function gene expression of zonula occludens-1 (*ZO-1*) and claudin-1 in goats. Differences in data were assessed by the one-way ANOVA with Tukey's test. (E) Inflammatory gene expression in the colon of goats. Differences in data were assessed by the one-way ANOVA with Tukey's test. (F) Differential operational taxonomic units (OTU) were selected using LEfSe analysis in the microbiota. When all samples were treated as independent, the Linear Discriminant Analysis score showed significant enrichment for taxa ($P < 0.05$ and $|LDA| > 3$). (G) Phylogenetic distribution of the most abundant cecum OTU354. The tree was generated using IQ-TREE (version 1.6.8) with the maximum likelihood method. (H) Fold changes of bacteria from cecum content using real-time PCR were determined for *B. acidifaciens* and *B. uniformis*. (I) Spearman correlation between short-chain fatty acids and OTU in early weaning strategies. Each spot color in the heatmap corresponds to the *R*-value of the spearman correlation analysis between microbial abundance and SCFA concentration, the green spot with a asterisk shows a significant positive correlation with $R > 0.6$ and $P < 0.05$, while the yellow spot with a asterisk indicates a significant negative correlation with $R < -0.6$ and $P < 0.05$. (J) Spearman correlation between gene and OTU in early weaning strategies. Each spot color in the heatmap corresponds to the *R*-value of the spearman correlation analysis between microbial abundance and gene abundance. The spot with a green asterisk indicates a significant positive correlation with $R > 0.6$ and $P < 0.05$, while the spot with a yellow asterisk shows a significant negative correlation with $R < -0.6$ and $P < 0.05$. Not significantly different (ns.) $P > 0.05$, *$P < 0.05$, **$P < 0.01$, and ***$P < 0.001$. D28 and D60 represent the goat kids were weaned from their mothers at 28 and 60 d.

2.11. Availability of data and materials

The 16S rRNA gene sequencing and RNA-seq data are available from the national center for biotechnology information (NCBI) under accessions PRJNA660305 and PRJNA660966, respectively.

3. Results

3.1. Goat growth performance and organ weights

The live body weight of the 2 groups was similar until 56 d of age, after which D28 goats became significantly heavier (2.84 ± 0.59 kg) until the end of the study (Fig. 1B). Moreover, there was no significant difference in the liver, spleen, and kidney organ indices between the 2 groups (Appendix Fig. 1A).

3.2. Serum parameters

D28 group showed reduced serum IL-1β and TNF-α (Fig. 1C) as well as the IgA and IgM levels (Fig. 1D), whereas IL-6 and IgG levels were not affected (Fig. 1C–D) compared with the D60 group. Glu levels in D28 group was significantly increased compared with the D60 group (Fig. 1E) but serum urea (Fig. 1E), TP, ALB, GLB, TC, and TG levels were not different between groups (Appendix Fig. 1B and C). Further evaluation of the indicators related to weaning stress and antioxidants in the serum, revealed that serum •OH, HIF-1β, Cor, Cort, DAO, GSH-Px, and SOD concentration in the D28 group were not significantly different to the D60 group (Appendix Fig. 1D–F).

3.3. The gene expression of inflammatory markers in the spleen

We conducted further gene expression analysis of inflammatory markers in the spleen by qPCR and found a significant upregulation of pro-inflammatory genes in the D60 group, including *TNF-α* and *IL-1β* (Fig. 1F). On the contrary, *IL-10* and cytokine synthesis inhibitor genes were downregulated in the D60 group relative to the D28 group (Fig. 1F).

3.4. Effects of different weaning strategies on the hindgut microbial composition and metabolites as well as colonic gene expression

In the D28 group, there was a significant increase in the concentration of propionate, butyrate, and valerate, whereas acetate, isobutyrate, and isovalerate were significantly decreased (Fig. 2A). At the same time, G protein–coupled receptor (*GPR*)*43,* the fatty acid receptor gene, was significantly upregulated in the colon of the early weaning group (Fig. 2B).

We observed a significant upregulation of colonic pro-apoptotic gene expression, with respect to *Bax*, caspase-9, and caspase-3 (Fig. 2C) and at the same time a decreased expression of the anti-apoptotic gene (*Bcl-2*) (Fig. 2C) in early-weaned goats. Early weaning also significantly decreased the expression of genes associated with the colonic barrier function, including *ZO-1* and claudin-1 (Fig. 2D). Similarly, early weaning significantly increased colonic proinflammatory gene expression of *IL-6*, decreased anti-inflammatory gene expression of *IL-10*, but did not affect the *IL-1β*, tumor necrosis factor (*TNF*)-*γ*, and *TNF-α* gene expression (Fig. 2E).

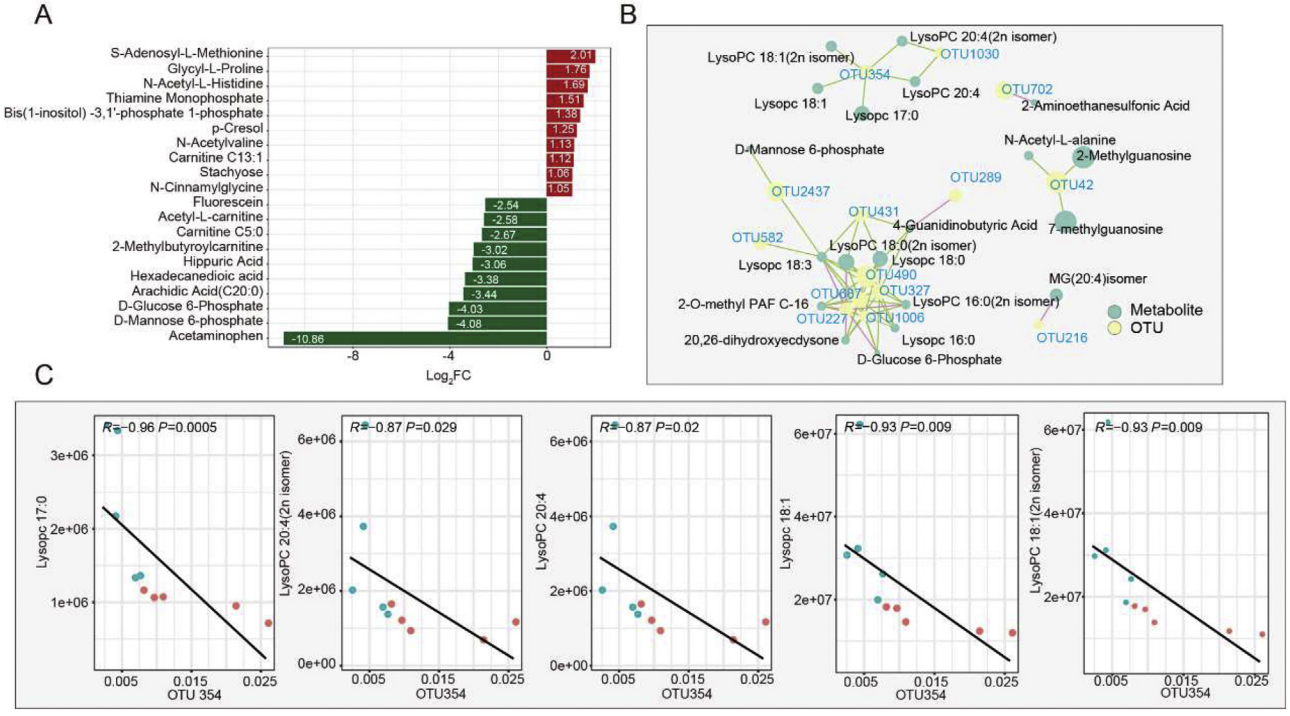

Fig. 3. Early weaning strategies alter hindgut luminal metabolite levels. (A) Differential metabolites bar chart in D60 vs. D28 group goats. The x-coordinate represents the log 2 value of the differential multiple, the y-coordinate represents the metabolite, the red color shows the significant upregulation in D28 group, and the green color indicates significant downregulation in D28 group. (B) Correlation between different operational taxonomic units (OTU) and different metabolites. The green circle color indicates the metabolites, and the yellow shows the OTU. The larger the circle, the greater the relative abundance of OTU or metabolites. The red line segment indicates significant positive correlation with $R > 0.7$ and $P < 0.05$, while the green line segment represents significant negative correlation with $R < -0.7$ and $P < 0.05$. (C) Spearman correlation between metabolites and OTU354 in early weaning strategies goats. The x-coordinate represents the relative abundance of OTU354, the y-coordinate shows the metabolite expression; the spot indicates the samples; the different colors represent different groups; and R indicates the correlation coefficient. D28 and D60 represent the goat kids were weaned from their mothers at 28 and 60 d.

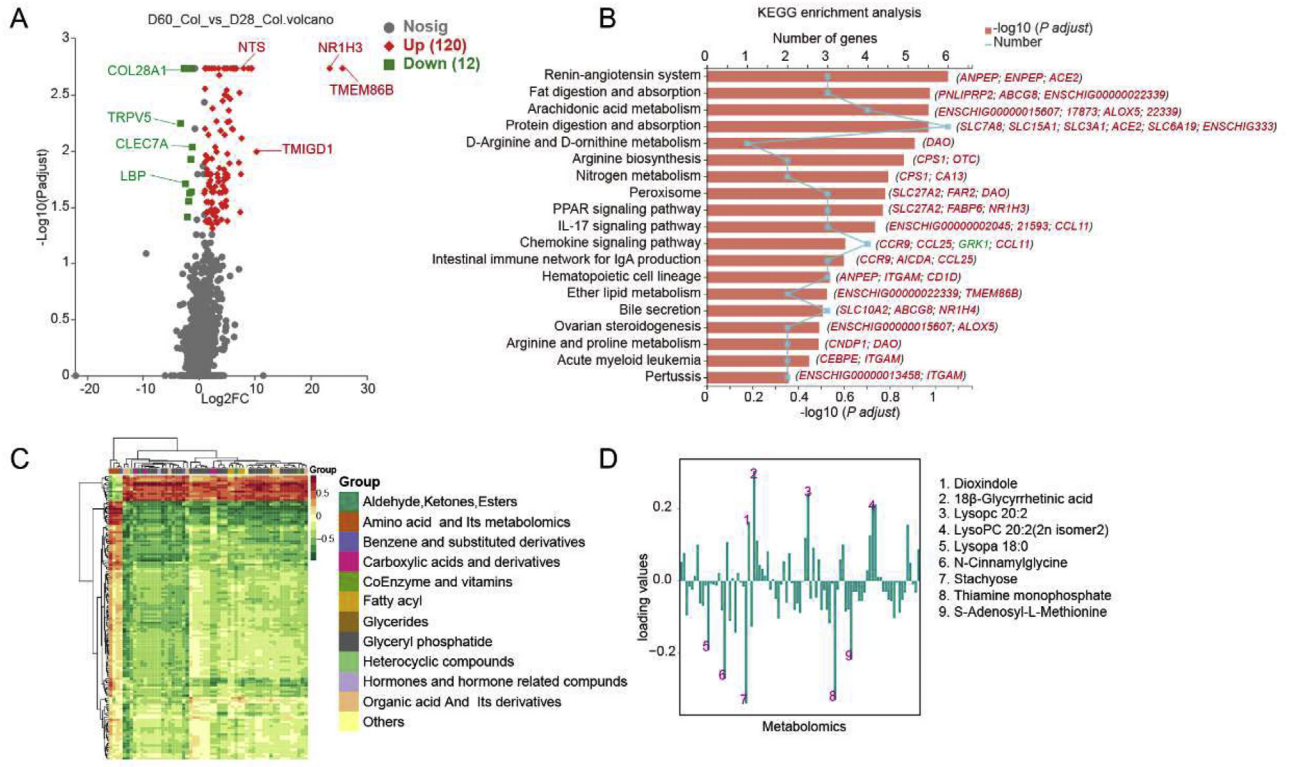

Fig. 4. Early weaning alters transcriptional profile of colonic epithelium. (A) Volcano plots for the RNA-seq analyses of D60 group vs. D28 group. The red circle represents upregulated differentially expressed genes (DEG), while the green represents the downregulated DEG. (B) The Kyoto Encyclopedia of Genes and Genomes enrichment analysis of DEG of D60 group vs. D28 group. The genes in each bar are the gene name involved in the pathway. The red gene name represents upregulated DEG, while the green represents downregulated DEG. (C) Spearman correlation heatmap between various metabolites and DEG of D28 and D60 groups. Different metabolites with correlation coefficients above 0.8. (D) The 2-way orthogonal partial least squares (O2PLS) metabolomic orthogonal loadings. Orthogonal part loadings obtained from an O2PLS fit with metabolomics and transcriptomics. The top 10 metabolites are highlighted. D28 and D60 represent the goat kids were weaned from their mothers at 28 and 60 d. *NTS* = neurotensin; *TMIGD1* = transmembrane and immunoglobulin domain containing 1; *NR1H3* = nuclear receptor subfamily 1 group H member 3; *TMEM86B* = transmembrane protein 86B; *LBP* = lipopolysaccharide binding protein; *CLEC7A* = C-type lectin domain containing 7A; *TRPV5* = transient receptor potential cation channel subfamily V member 5; *COL28A1* = collagen type XXVIII Alpha 1 chain; *ANPEP* = alanyl aminopeptidase, *ENPEP* = glutamyl aminopeptidase; *ACE2* = angiotensin converting enzyme 2; *PNLIPRP2* = pancreatic lipase related protein 2; *ABCG8* = ATP binding cassette subfamily G member 8; *ALOX5* = arachidonate 5-lipoxygenase; *SLC7A8* = solute carrier family 7 member 8; *SLC15A1* = solute carrier family 15 member 1; *SLC3A1* = solute carrier family 3 member 1; *SLC6A19* = solute carrier family 6 member 19; *DAO* = D-amino acid oxidase; *CPS1* = carbamoyl-phosphate synthase 1; *OTC* = ornithine transcarbamylase; *CA13* = carbonic anhydrase 13; *FAR2* = fatty acyl-CoA reductase 2; *CEBPE* = CCAAT enhancer binding protein epsilon; *ITGAM* = integrin subunit alpha M; *CNDP1* = carnosine dipeptidase 1; *ALOX5* = arachidonate 5-lipoxygenase; *SLC10A2*= solute carrier family 10 member 2; *NR1H4* = nuclear receptor subfamily 1 group H member 4; *CCR9* = C-C motif chemokine receptor 9; *CCL25* = C-C motif chemokine ligand 25; *CCL11* = C-C motif chemokine ligand 11; *FABP6* = fatty acid binding protein 6.

The 16S rRNA gene sequencing of caecal microbial DNA revealed no significant difference in α-diversity (via Sob, Chao, Shannon and Coverage index) between groups (Appendix Fig. 2A), but a significant difference in β-diversity (Appendix Fig. 2B). We analyzed the degree of bacterial taxonomic similarity at the phylum level to assess the overall composition of the bacterial communities (Appendix Fig. 2C), which revealed that there was no significant difference in the relative abundance within the 2 groups. Notably, genus-level analysis in the D28 group showed that there was a significant increase in the abundance of *Eubacterium*, *Mogibacterium*, *Anaerorhabdus,* and *U_Peptococcaceae 1* (Appendix Fig. 2D). The OTU-level analysis showed that early weaning promoted a significant increase in the relative abundance of OTU2469 (Bacteroidetes), OTU354 (*U_Bacteroidales*), OTU314 (*Clostridium_IV*), and OTU1829 (Ruminococcaceae) (Fig. 2F), and decreased the abundance of OTU370 (*U_Bacteroidales*), OTU469 (*Alistipes*), OTU537 (*U_Clostridiales*), OTU442 (*U_Porphyromonadaceae*), and OTU672 (*U_Ruminococcaceae*) (Fig. 2F, Appendix Fig. 2E). Phylogenetic analysis showed that *B. acidifaciens* was the most abundant OTU354 (Fig. 2G), and OTU370 and OTU387 were phylogenetically related to *B. uniformis* (Appendix Fig. 2F). Therefore, we used all the identified *U_Bacteroidales* data together and observed that *U_Bacteroidales* contributes to more than 11% of the total microbiota abundance. In order to verify the results from the LEfSe data outputs, real-time PCR was performed with primers specific for the species *B. acidifaciens* and *B. uniformis*. The results of PCR validation confirmed the findings observed in the sequencing data. Specifically, *B. acidifaciens* was found to be significantly increased in the caecal of the D28 group (Fig. 2H), while *B. uniformis* was significantly higher in the caecal of the D60 group (Fig. 2H).

The correlation of gene expression levels, SCFA, and differential OTU was estimated to determine if the cecum microbiota imbalance has any relation to the intestinal barrier integrity and inflammatory function of early-weaned goats. There were strong correlations between OTU354 and intestinal barrier integrity and inflammatory function-related genes and SCFA (Fig. 2I–J). OTU354 was positively correlated with propionate ($R = 0.75$, $P = 0.01$), butyrate ($R = 0.98$, $P = 0.001$), valerate ($R = 0.73$, $P = 0.01$), caspase-3 ($R = 0.68$, $P = 0.02$), *Bax* ($R = 0.84$, $P = 0.002$), *IL-6* ($R = 0.67$, $P = 0.03$), *IL-1β* ($R = 0.83$, $P = 0.002$), and *GPR43* ($R = 0.75$, $P = 0.01$), and negatively correlated with isobutyrate ($R = -0.90$, $P = 0.003$), isovalerate ($R = -0.89$, $P = 0.005$), *ZO-1* ($R = -0.82$, $P = 0.003$), claudin-1 ($R = -0.71$, $P = 0.02$), *Bcl_2* ($R = -0.73$, $P = 0.01$), and *IL-10* ($R = -0.74$, $P = 0.01$) (Fig. 2I–J).

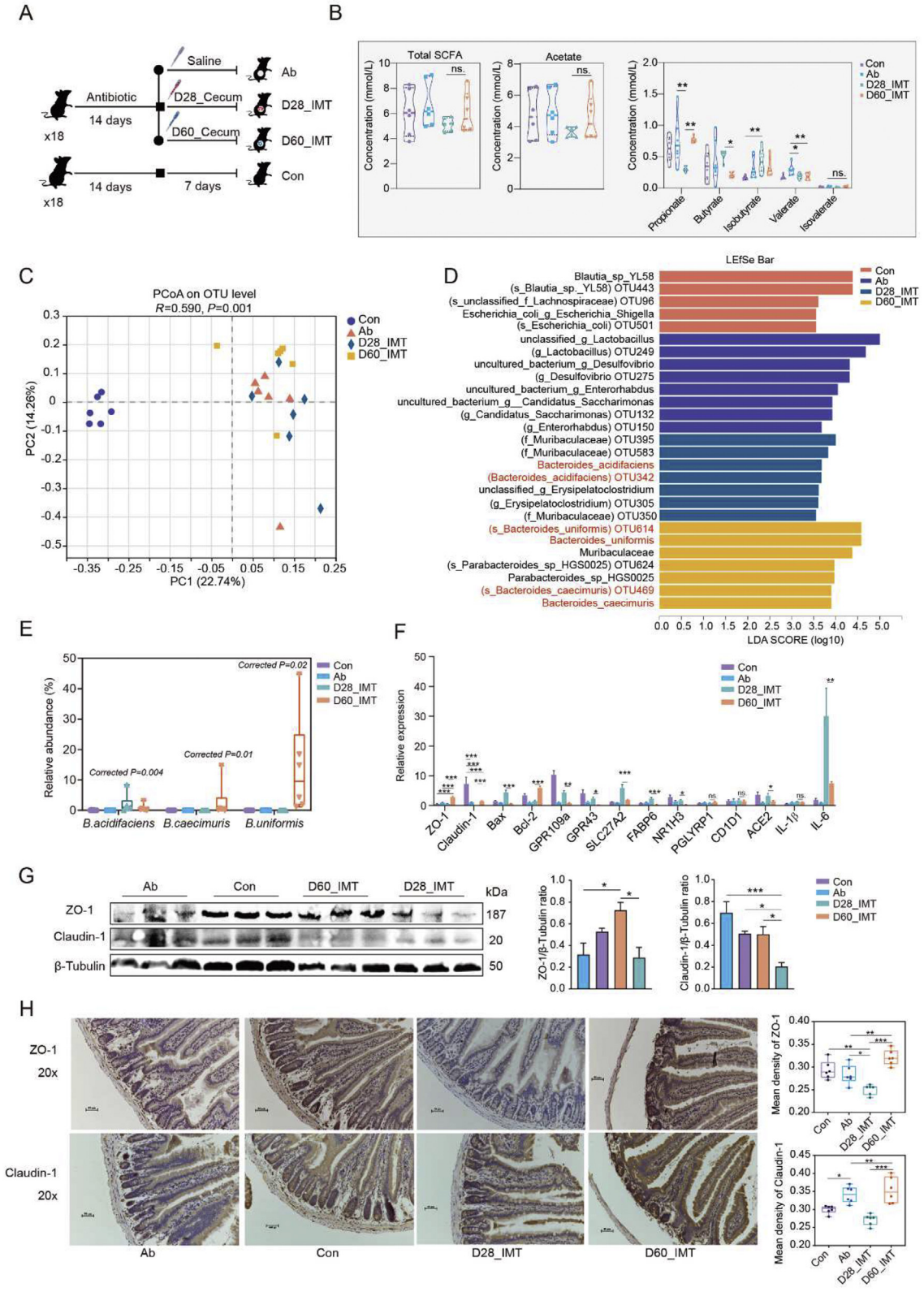

Fig. 5. Early weaning weakening barrier function are transferable by intestinal microbiota transplantation (IMT). (A) The design paradigm. (B) Fermentation parameters of the mouse cecum content. One-way ANOVA with Tukey's test was used to assess the data differences. (C) Principle coordinate analysis (PCoA) plot based on the Bray–Curtis dissimilarities of mouse cecum microbiota in Con, Ab, D28_IMT, and D60_IMT groups ($n = 6$ individuals/group). The ANOSIM statistic compares the mean of ranked dissimilarities between groups to the mean of ranked dissimilarities within groups. (D) Differential bacterial taxonomy selected using the linear discriminant analysis effect size analysis with linear discriminant analysis score in cecum microbiota > 3.5. (E) Abundance is represented as the operational taxonomic units (OTU) proportions classified at a species level. Data are represented as means ± SEM ($n = 6$ per group). One-way ANOVA with Tukey's test was used to assess the data differences. (F) Gene expression in mice' colon. Data are shown as means ± SEM ($n = 6$ per group). One-way ANOVA with Tukey's test was used to assess the data differences. (G) Representative Western blot brands and density analysis of zonula occludens-1 and claudin-1 in the colon tissue. One-way ANOVA with Tukey's test was used to assess the data differences. (H) Representative immunohistochemical images and

3.5. Early weaning strategies affect the hindgut luminal metabolite levels

Untargeted metabolome profiles were generated on cecum content samples using an LC-ESI-MS/MS system to assess hindgut metabolic alternation content in response to the hindgut microbiota remodeled by early weaning. According to the orthogonal partial least squares–discrimination analysis (OPLS-DA), distinct metabolites clustering was evident in both D28 and D60 goats (Appendix Fig. 3A). A total of 11 metabolites in the D28 group were increased, including S-adenosyl-L-methionine, glycyl-L-proline, N-acetyl-L-histidine, thiamine monophosphate, bis(1-inositol)-3,1′-phosphate-1-phosphate, p-cresol, N-acetylvaline, carnitine C13:1, 2-methylguanosine, cinnamyl glycine, and stachyose (Fig. 3A; Appendix Table 4), whereas 78 metabolites were decreased compared to the D60 group (Appendix Fig. 3B). Significantly regulated metabolites in the 2 groups were determined using variable importance in projection (VIP) > 1 and absolute Log_2FC (fold change) $\geq$ 1. We found that some of the reduced metabolites, including lysophosphatidylcholine (LysoPC) 20:3, LysoPC 20:3 (2n isomer), all-trans-13,14-dihydroretinol, LysoPC 20:1 (2n isomer), acetaminophen, LysoPC 18:1, LysoPC 17:0, LysoPC 20:1, and LysoPC 18:1 (2n isomer) had VIP values $\geq$ 2 (Appendix Fig. 3C; Appendix Table 4). The Kyoto Encyclopedia of Genes and Genomes (KEGG) compound database generated the KEGG enrichment to describe the effect of early weaning on these responsive metabolites and revealed that the thyroid hormone synthesis, taurine, and hypotaurine metabolism, phosphatidylinositol signaling, inositol phosphate metabolism, glycerophospholipid metabolism, galactose metabolism, fructose, and mannose metabolism, Fc gamma R–mediated phagocytosis, fat digestion and absorption, and amino sugar and nucleotide sugar metabolism were the most significantly affected pathways (Appendix Fig. 3D). We calculated Spearman's rho coefficients of the 4 phylotypes (OTU354, OTU490, OTU42, and OTU216) to probe the associations between cecum microbiota and metabolome. Coefficients greater than 0.7 with a *P*-value less than 0.05 were considered significant. We found that OTU354 negatively correlated with lysophosphatidylcholines (LysoPC) such as LysoPC 18:1 (2n isomer), LysoPC 17:0, LysoPC 18:1, LysoPC 20:4 (2n isomer), and LysoPC 20:4 (Fig. 3B–C).

3.6. Early weaning alters the transcriptional profile of the colonic epithelium

We performed transcriptome sequencing on colonic epithelium samples taking into account the interactions between microbiota and host together with the changes of cecum microbiota and metabolites in early-weaned goats to study the effect of microbiota and metabolites on substance metabolism and signal transduction in colonic epithelium. A total of 86.67 Gb of data was obtained using RNA-seq of 10 colonic epithelial samples. On average there were 66.85 million high-quality, paired reads generated per sample (mean ± SD = 66, 856, 329 ± 3,601,070) from RNA-seq and the overall read alignment rate to the *Capra_hircus* reference genome was more than 93.98%.

Significantly differentially expressed genes (DEG) in the 2 groups were determined using |log2FC| $\geq$ 1 and *P* adjust < 0.05 by DESeq2 (V1.24.0). In total, 132 genes were expressed differentially, of which 120 were upregulated, and 12 were downregulated (Fig. 4A). The detailed information of each DEG is shown in Appendix Table 5. The DEG were enriched in 106 KEGG pathways. Among them, a total of 12 pathways were screened, including chemokine signaling pathway, involved in C–C motif chemokine receptor 9 (*CCR9*), C–C motif chemokine ligand 25 (*CCL25*), G protein-coupled receptor kinase 1 (*GRK1*), and *CCL11*, *IL-17* signaling pathway, peroxisome proliferators-activated receptor (*PPAR*) signaling pathway, involved in solute carrier family 27 member 2 (*SLC27A2*), fatty acid binding protein 6 (*FABP6*), and nuclear receptor subfamily 1 group H member 3 (*NR1H3*), peroxisome, nitrogen metabolism, arginine biosynthesis, D-arginine, and D-ornithine metabolism, protein digestion and absorption, arachidonic acid metabolism, fat digestion and absorption, renin-angiotensin system, involved in alanyl aminopeptidase, membrane (*ANPEP*), glutamyl aminopeptidase (*ENPEP*), and angiotensin converting enzyme 2 (*ACE2*), and the intestinal immune network for IgA production, involved in *CCR9*, activation induced cytidine deaminase (*AICDA*), and *CCL25*) (Fig. 4B).

Spearman's coefficients between the DEG and cecum luminal metabolites were calculated, and coefficients greater than 0.8 with a *P*-value < 0.05 were considered significant. One hundred and twenty upregulated genes and glyceryl phosphatide (mainly including LysoPC) and 12 down-regulated genes positively correlated with amino acids and their metabolites, benzene, and substituted derivatives, respectively (Fig. 4C). All differentially expressed genes and metabolites were selected to establish the 2-way orthogonal partial least squares (O2PLS) model, and essential metabolites that potentially modulated gene expression was screened out to further evaluate the effect of hindgut differential metabolites on the expression of colonic epithelial genes. Nine key metabolites, including dioxindole, 18β-glycyrrhetinic acid, LysoPC 20:2, LysoPC 20:2 (2n isomer 2), LysoPC 18:0, 6 N-cinnamylglycine, stachyose, thiamine monophosphate, and S-adenosyl-L-methionine were screened (Fig. 4D). Spearman's correlation coefficient was calculated between the concentration of serum inflammatory markers and metabolite profiles in each group. The results showed a positive association between TNF-α, IL-6, and IL-1β with LysoPC products, respectively (Appendix Fig. 4).

3.7. Early weaning weakening barrier function is transferable by IMT

The cecum microbiota from D28 and D60 groups was transferred to bacterial-restricted C57/6J mice (Fig. 5A). D28_IMT receivers expressed decreased cecum propionate and increased butyrate concentrations compared with D60_IMT receivers (Fig. 5B). We conducted 16S rRNA gene sequencing to examine the cecum bacterial composition to confirm that fecal transplantation modulates the gut microbiota. PCoA revealed that there was a significant difference in the microbial community in the Ab, Con, D28_IMT, and D60_IMT treatment groups ($R = 0.590$, $P = 0.001$; D28_IMT vs. D60_IMT, $R = 0.30$, $P = 0.018$; ANOSIM; Fig. 5C). The cecum microbiota transfer resulted in a significant increase in the relative abundance of *B. acidifaciens* in the D28_IMT receivers (Fig. 5D), while in D60_IMT receivers the relative abundance of *B. uniformis* and *Bacteroides caecimuris* was significantly increased (Fig. 5D). Interestingly, *B. acidifaciens*, *B. caecimuris,* and *B. uniformis* were not identified in the Con and Ab groups (Fig. 5E). The mRNA expression level of genes associated with barrier function, apoptosis, and proinflammatory response in the colon of Ab, Con, D28_IMT, and D60_IMT treatment groups was further investigated.

quantitative analysis of zonula occludens-1 and claudin-1 protein in jejunum tissue ($n = 6$ per group; scale bar, 50 μm). One-way ANOVA with Tukey's test was used to assess the data differences. Not significantly different (ns) $P > 0.05$, $^{*}P < 0.05$, $^{**}P < 0.01$, and $^{***}P < 0.001$. Con, a control group (without any treatment); Ab, an antibiotic group, which received sterile saline via gavage after antibiotic treatment stopped; D28_IMT, a group that was transplanted with group D28 cecum microbiota after antibiotic treatment stopped; and D60_IMT, a group that was transplanted with D60 cecum microbiota after antibiotic treatment stopped.

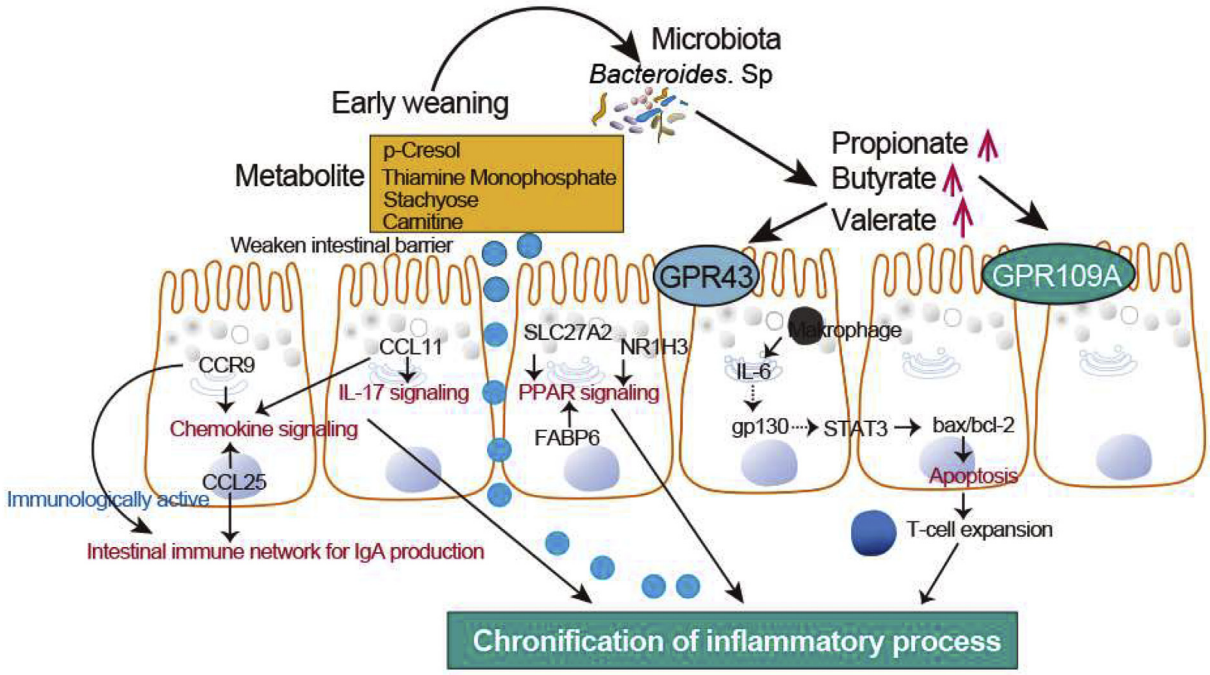

Fig. 6. Hindgut microbiota and metabolites media colon inflammatory process. Gut microbes, especially *Bacteroides* sp. and bacteria-derived metabolites were identified using short-chain fatty acids (propionate, butyrate, and valerate) and p-cresol, carnitine. Altered colon metabolic dysfunction was involved in the renin-angiotensin system pathway, *IL-17* signaling pathway, and peroxisome proliferators-activated receptor signaling pathway. *GPR43* = G protein–coupled receptor 43; *GPR109A* = G protein–coupled receptor 109A; *CCR9* = C-C motif chemokine receptor 9; *CCL25* = C-C motif chemokine ligand 25; *CCL11* = C-C motif chemokine ligand 11; *SLC27A2* = solute carrier family 27 member 2; *NR1H3* = nuclear receptor subfamily 1 group H member 3; *FABP6* = fatty acid binding protein 6; *gp130* = interleukin-6 receptor subunit beta; *STAT3* = signal transducer and activator of transcription 3; *Bax* = B-cell lymphoma associated X; *Bcl-2* = B-cell lymphoma-2.

There was a significant decrease in the mRNA expression of *ZO-1,* claudin-1 and *Bcl-2* in the D28_IMT group compared to the D60_IMT group (Fig. 5F), while that of *Bax*, *GPR109A*, *GPR43*, *SLC27A2*, *FABP6*, *NR1H3*, *ACE2,* and *IL-6* were significantly increased in the D28_IMT group compared to the D60_IMT group (Fig. 5F). To determine whether the IMT is associated with intestinal and hindgut barrier function, we conducted immunohistochemistry and Western blot analysis to evaluate the protein expression associated with the gut barrier function. The D28_IMT group had a decreased ZO-1 and claudin-1 expression in their jejunum compared with the D60_IMT group (Fig. 5G). Consistently, the colon tissue Western blot results illustrated that the expression of the 2 major tight junction proteins decreased significantly in the D28_IMT group, including ZO-1 ($P < 0.05$) and claudin-1 ($P < 0.05$) compared to the D60_IMT group (Fig. 5H).

4. Discussion

The purpose of this study was to identify the functional relationships between early weaning and the hindgut microbiota, emphasizing a potential microbial modulation of the host's immune response to early weaning stress. Two groups of female goats (either weaned late at 60 d or early at 28 d postpartum) received a standardized post-weaning feeding from 28 d until 75 d postpartum. We demonstrated using multi-omics methodology of amplicon sequencing together with metabolomic profiling and RNA-seq analysis, that early weaning modulated the hindgut metabolome, thereby directly affecting the gut physiology of goats. We found that early weaning increased the hindgut abundance of *Bacteroides* spp., and increased the luminal concentrations of propionate, butyrate, and valerate. In response to early weaning stress, the expression of *Bax*, *GPR109*A, *GPR43*, *SLC27A2*, *FABP6*, *NR1H3*, *ACE2*, and *IL-6* genes were significantly upregulated, and impaired glycerophospholipid metabolism in the hindgut was evident. Our findings demonstrate that early weaning weakened the hindgut epithelial barrier by disrupting the integrity of the colon mucosa through the upregulation of the *IL-17* signaling pathway, *PPAR* signaling pathway, and chemokine signaling pathway (Fig. 6).

Earlier studies have shown a high abundance of *B. acidifaciens* in trinitrobenzene sulfonic acid (TNBS) and dextran sulfate sodium (DSS)-induced mouse colitis models (Munyaka et al., 2016; Schwab et al., 2014), hence it has been classified as a specific biomarker for colitis (Berry et al., 2013). Berry et al. (2013) have shown that *B. acidifaciens* can degrade the mucin in the intestine and promote intestinal microbial malnutrition and intestinal inflammation (Berry et al., 2013; Busbee et al., 2020). Our results found that there is a high OTU354 (*B. acidifaciens*) abundance in the hindguts of early-weaned goats. *B. acidifaciens* positively correlated with the apoptosis gene *Bax* expression, and negatively correlated with barrier genes, *ZO-1* and claudin-1. Interestingly, *B. acidifaciens* was not identified in the mice cecum in the Con and Ab groups, but it had a high abundance in the cecum of the D28_IMT group. However, compared to the D60_IMT group, the intestinal inflammatory factor *IL-6* was significantly up-regulated, and the intestinal barrier protein ZO-1 and claudin-1 were significantly down-regulated in the jejunum and colon of the D28_IMT group. Transplantation of cecum microbes of early-weaned goats can significantly cause hindgut inflammation in mice and is closely related to the high *B. acidifaciens* abundance. Studies have shown that *B. acidifaciens* can increase IL-6 and IL-10 production by enhancing MHC class II molecule expression and also co-stimulating molecules (i.e., CD80 and CD86) on antigen-presenting cells (Yang et al., 2017). Feeding *B. acidifaciens* resulted in fat oxidation activation through the bile acid-TGR5-PPARa axis in adipose tissues, leading to high energy use. *B. acidifaciens* also activates *DPP-4* in the gut, subsequently increasing *GLP-1*, which can contribute to glucose homeostasis

(Wang et al., 2020). *B. acidifaciens* is closely related to down-regulated intestinal barrier proteins ZO-1 and claudin-1 of the colon (Berry et al., 2013). It is important to further explore its mechanism on targeting bacteriocins and pro-inflammatory factors.

Furthermore, previous studies have shown that breastfeeding can increase the *B. uniformis* abundance in the offspring's gut (Sánchez et al., 2011), which is essential for the intestinal immunity development (Sánchez et al., 2011). *B. uniformis* use can also improve the macrophages and dendritic cells (DCs) immune functions, thus improving their ability to produce cytokines in response to lipopolysaccharide, and restore the DCs ability to identify antigens and stimulate the T lymphocytes proliferation (Cano et al., 2012). Feeding mice on *B. uniformis* for a long time has potential benefits; for example, it changes the gut microbial community composition and promotes potentially beneficial bacteria (Gómez del Pulgar et al., 2020). Our results also showed no trace of *B. uniformis* before IMT; however afterwards, it was significantly enriched in the hindgut of the D60 group goat kids. The result of this enrichment appeared to be a proper barrier function. Reducing acyl carrier protein expression, which is a basic component necessary for the biosynthesis of lipopolysaccharide by gram-negative bacteria, and its growth and survival is another potential probiotic function of *B. uniformis* (Masoudi et al., 2014). Lipopolysaccharide can promote the expression of pro-inflammatory cytokines, thereby causing, for example, chronic low-grade inflammation in obesity (Cani et al., 2007; Wang et al., 2020). Therefore, our results suggest *B. uniformis* may have a dampening effect on the gut inflammatory status.

Butyric acid provides about 70% of the energy for normal intestinal epithelial cells, and promotes gut cell growth and proliferation at low concentrations. In strong contrast, butyric acid can inhibit gut cell proliferation and promote cell apoptosis at high concentrations (more than 5 mmol/L) as HDACi (Gonçalves and Martel, 2013), which is relevant for the progression of intestinal tumor cells (Lazarova and Bordonaro, 2016), for example. In the present study we observed a 5-fold higher butyrate concentration in the hindgut lumen and an associated up-regulation of pro-inflammatory pathways in the mucosal cells of D28 goat kids. This adds another piece to the puzzle of the detrimental effects of early weaning on gut health. This increase in butyric acid concentration could be related to the higher abundance of *B. acidifaciens,* which is in line with earlier studies (Romaní-Pérez et al., 2017; Yang and Kweon, 2016).

Our colonic epithelial transcriptome results indicate that the DEG *ACE2* is involved in the stress-related renin-angiotensin system pathway and protein digestion and absorption. A previous study showed that *ACE2* upregulation in IBD is associated with inflammation and anti-cytokine therapy response (Potdar et al., 2020), while upregulated *ACE2* in the colon is associated with deteriorated clinical results in Crohn's disease (Toyonaga et al., 2021). *ACE2* regulates the neutral amino acid transporter B^0-type amino acid transporter 1 (B^0AT1) expression, thus controlling tryptophan-associated intestinal inflammation and nutritional status (Ferreira-Duarte et al., 2020). Moreover, the DEG *CCL11* is involved in the IL-17 signaling pathway and chemokine signaling pathway. A previous study showed that CCL11 plays a critical role in regulating eosinophil recruitment in colonic eosinophilic disease (Ahrens et al., 2008), and the upregulated association of CCL11 between aberrant immune-physiological responses of the gastrointestinal tract (Adar et al., 2014); especially colonic inflammation (Jeziorska et al., 2001). Therefore, we conclude that early weaning mediates the upregulation of proinflammatory genes in the colonic epithelium, the majority of which is involved in the renin-angiotensin system pathway, *IL-17* signaling pathway, and *PPAR* signaling pathway. Long-term experiments should be conducted to further determine its effect on the growth performance of animals.

It was shown that early weaning significantly upregulated the p-cresol abundance in the hindgut, which is considered a metabolic troublemaker and a genotoxic luminal bacterial metabolite in colonic epithelial cells (Andriamihaja et al., 2015). It also caused DNA damage in a dose-dependent manner and affected cell cycle kinetics in HT29 and Caco-2 cells (Al Hinai et al., 2019). Early weaning also significantly down-regulated the acetaminophen abundance in the hindgut. Acetaminophen, a nonsteroidal anti-inflammatory drug with potential antipyretic and analgesic actions (Bradley et al., 1991), protects the gastric mucosa against erosive damage by not only increasing mucosal prostaglandin synthesis but possibly also through other mechanisms, such as scavenging of free hydroxyl radicals (Botting, 2000). Besides, LysoPC abundance was associated with colon dysfunction. Several pieces of evidence have shown that LysoPC plays a major role in the animal atherosclerosis development (Chen et al., 1997; Marathe et al., 2001; Ylä-Herttuala et al., 1989), inducing the release of adhesion molecules and chemokines release, thereby further increasing pro-inflammatory activity (Kume et al., 1992; Kume and Gimbrone, 1994; Takahara et al., 1996). LysoPC participates in the inflammation pathogenesis, acts as a chemokine for monocytes and T cells, and has pro-inflammatory properties, after its absorption in the blood. Our serum analysis results showed that serum *IL-1β* and *TNF-α* levels in the D60 group were significantly increased. The previous study found that LysoPC (16:0), LysoPC (18:1), and LysoPC (20:4) are the most common LysoPC produced by the effect of endothelial lipase on high-density lipoproteins, promoting *IL-8* synthesis. Therefore, intestinal bacteria can activate macrophages and epithelial cells, leading to increased LysoPC levels (Zhang et al., 2012). LysoPC up-regulation indicates not only the possibility of an impaired inflammatory response, but also microbiota disturbance. The sensitivity to specific bacteria (such as *Desulfovibrio_piger_HAQ-6*) is also increased. The detailed mechanism of action should be investigated.

5. Conclusions

In conclusion, our findings show that the hindgut microbiota is essential in colon inflammatory response regulation to early weaning. Hindgut microbiota of early weaning goat was involved in down-regulating the intestinal barrier gene expression, promoting the inflammatory factor expression, and promoting the colon epithelial cell apoptosis. Early weaning promoted colon metabolic dysfunction by affecting the renin-angiotensin system pathway, *IL-17* signaling pathway, and *PPAR* signaling pathway. Weaning at 60 d after birth could increase the relative abundance of *B. uniformis*, and improving the colon epithelial barrier gene expression. Furthermore, our data demonstrate a link between early weaning and hindgut metabolic health. This study also has implications for the further development of early weaned goats, since they are at higher risk of accelerated early growth and metabolic dysfunction and might benefit from revisiting probiotics added in artificial feed or milk. In summary, this study highlights the gut microbial imbalance as an important risk for early weaning interventions and suggests that modulating probiotics intake after weaning may hold promise as a strategy for gut inflammatory prevention. Furthermore, based on our mice data, these results are transferable to other mammalian species.

Author contributions

Yulin Chen: Conceptualization, Project administration, Funding acquisition, Writing – review & editing. **Ke Zhang:** Conceptualization, Methodology, Investigation, Visualization, Supervision,

Writing – original draft. **Yangbin Xu:** Resources, Investigation. **Bo Zong:** Investigation. **Mengmeng Guo:** Resources, Investigation. Ting Zhang: Resources, Investigation. Langda Suo: Conceptualization, Investigation. **Shuhong Huang:** Visualization. **Baohua Ma:** Conceptualization. **Daniel Brugger:** Writing – review & editing. **Xiaolong Wang:** Conceptualization, Writing – review & editing. Yujiang Wu: Conceptualization, Investigation, Funding acquisition. **Yuxin Yang:** Conceptualization, Methodology, Writing – review & editing, Funding acquisition.

Declaration of competing interest

We declare that we have no financial and personal relationships with other people or organizations that can inappropriately influence our work, and there is no professional or other personal interest of any nature or kind in any product, service and/or company that could be construed as influencing the content of this paper.

Acknowledgements

This work was financially supported by Qinghai Province Key R&D and Transformation Plan (2020-NK-127), Tibet Science and Technology Department's "13th Five-Year Plan" Major Agriculture Project (XZ201901NA02), the Key Technology R&D Program of Xinjiang Groups (2020AB016), Science and Technology Program of Tibet (XZ202001YD0017C), Agriculture Research System of China (CARS-39-12).

Supplementary data

Supplementary data to this article can be found online at https://doi.org/10.1016/j.aninu.2022.04.004.

References

Adar T, Shteingart S, Ya'acov AB, Shitrit AB-G, Goldin E. From airway inflammation to inflammatory bowel disease: eotaxin-1, a key regulator of intestinal inflammation. Clin Immunol 2014;153:199–208.
Ahrens R, Waddell A, Seidu L, Blanchard C, Carey R, Forbes E, et al. Intestinal macrophage/epithelial cell-derived CCL11/eotaxin-1 mediates eosinophil recruitment and function in pediatric ulcerative colitis. J Immunol 2008;181:7390–9.
Al Hinai EA, Kullamethee P, Rowland IR, Swann J, Walton GE, Commane DM. Modelling the role of microbial p-cresol in colorectal genotoxicity. Gut Microb 2019;10:398–411.
Andriamihaja M, Chaumontet C, Tome D, Blachier F. Butyrate metabolism in human colon carcinoma cells: implications concerning its growth-inhibitory effect. J Cell Physiol 2009;218:58–65.
Andriamihaja M, Lan A, Beaumont M, Audebert M, Wong X, Yamada K, et al. The deleterious metabolic and genotoxic effects of the bacterial metabolite p-cresol on colonic epithelial cells. Free Radic Biol Med 2015;85:219–27.
Artis D. Epithelial-cell recognition of commensal bacteria and maintenance of immune homeostasis in the gut. Nat Rev Immunol 2008;8:411–20.
Belanche A, Cooke J, Jones E, Worgan H, Newbold C. Short-and long-term effects of conventional and artificial rearing strategies on the health and performance of growing lambs. Animal : Int J Animal Biosc 2019;13:740–9.
Berry D, Stecher B, Schintlmeister A, Reichert J, Brugiroux S, Wild B, et al. Host-compound foraging by intestinal microbiota revealed by single-cell stable isotope probing. Proc Natl Acad Sci Unit States Am 2013;110:4720–5.
Botting RM. Mechanism of action of acetaminophen: is there a cyclooxygenase 3? Clin Infect Dis 2000;31:S202–10.
Bradley JD, Brandt KD, Katz BP, Kalasinski LA, Ryan SI. Comparison of an antiinflammatory dose of ibuprofen, an analgesic dose of ibuprofen, and acetaminophen in the treatment of patients with osteoarthritis of the knee. N Engl J Med 1991;325:87–91.
Bravo AG, Zopfi J, Buck M, Xu J, Bertilsson S, Schaefer JK, et al. Geobacteraceae are important members of mercury-methylating microbial communities of sediments impacted by waste water releases. ISME J 2018;12:802–12.
Busbee PB, Menzel L, Alrafas HR, Dopkins N, Becker W, Miranda K, et al. Indole-3-carbinol prevents colitis and associated microbial dysbiosis in an IL-22–dependent manner. JCI insight 2020;5.
Byndloss MX, Olsan EE, Rivera-Chávez F, Tiffany CR, Cevallos SA, Lokken KL, et al. Microbiota-activated PPAR-γ signaling inhibits dysbiotic Enterobacteriaceae expansion. Science 2017;357:570–5.
Cani PD, Amar J, Iglesias MA, Poggi M, Knauf C, Bastelica D, et al. Metabolic endotoxemia initiates obesity and insulin resistance. Diabetes 2007;56:1761–72.
Cano PG, Santacruz A, Moya Á, Sanz Y. Bacteroides uniformis CECT 7771 ameliorates metabolic and immunological dysfunction in mice with high-fat-diet induced obesity. PLoS One 2012;7:e41079.
Chen L, Liang B, Froese D, Liu S, Wong J, Tran K, et al. Oxidative modification of low density lipoprotein in normal and hyperlipidemic patients: effect of lysophosphatidylcholine composition on vascular relaxation. J Lipid Research 1997;38:546–53.
Council NR, Nutrient N. Requirements of goats: angora, dairy, and meat goats in tempera tropical countries. Washington: National Research Council, National Academy Press; 1981.
De Clercq NC, Groen AK, Romijn JA, Nieuwdorp M. Gut microbiota in obesity and undernutrition. Adv Nutr 2016;7:1080–9.
Ferreira-Duarte M, Estevinho MM, Duarte-Araújo M, Magro F, Morato M. Unraveling the role of ACE2, the binding receptor for SARS-CoV-2, in inflammatory bowel disease. Inflamm Bowel Dis 2020;26:1787–95.
Fukata M, Arditi M. The role of pattern recognition receptors in intestinal inflammation. Mucosal Immunol 2013;6:451–63.
Gómez del Pulgar EM, Benítez-Páez A, Sanz Y. Safety assessment of Bacteroides uniformis CECT 7771, a symbiont of the gut microbiota in infants. Nutrients 2020;12:551.
Gonalves P, Martel F. Butyrate and colorectal cancer: the role of butyrate transport. Curr Drug Metabol 2013;14:994–1008.
Gonçalves P, Martel F. Butyrate and colorectal cancer: the role of butyrate transport. Curr Drug Metabol 2013;14:994–1008.
Guilloteau P, Martin L, Eeckhaut V, Ducatelle R, Zabielski R, Van Immerseel F. From the gut to the peripheral tissues: the multiple effects of butyrate. Nutr Res Rev 2010;23:366–84.
Jeziorska M, Haboubi N, Schofield P, Woolley DE. Distribution and activation of eosinophils in inflammatory bowel disease using an improved immunohistochemical technique. J Pathol: J Pathol Soc Great Britain Ireland 2001;194:484–92.
Kosior-Korzecka U, Wojcik M, Longo V, Puzio I, Nowakiewicz A, Patkowski K, et al. Changes in growth hormone secretion and leptin receptor mRNA expression under the influence of leptin and adrenocorticotropin in pituitary cells of early weaned Ewe lambs. J Physiol Pharmacol 2019;70:515–24.
Kume N, Cybulsky M, Gimbrone M. Lysophosphatidylcholine, a component of atherogenic lipoproteins, induces mononuclear leukocyte adhesion molecules in cultured human and rabbit arterial endothelial cells. J Clin Invest 1992;90:1138–44.
Kume N, Gimbrone MA. Lysophosphatidylcholine transcriptionally induces growth factor gene expression in cultured human endothelial cells. J Clin Invest 1994;93:907–11.
Lawley B, Tannock GW. Analysis of 16S rRNA gene amplicon sequences using the QIIME software package, Oral Biology, Springer. 2017. p. 153–63.
Lazarova DL, Bordonaro M. Vimentin, colon cancer progression and resistance to butyrate and other HDACis. J Cell Mol Med 2016;20:989–93.
Lei Y, Zhang K, Guo M, Li G, Li C, Li B, et al. Exploring the spatial-temporal microbiota of compound stomachs in a pre-weaned goat model. Front Microbiol 2018;9:1846.
Li B, Zhang K, Li C, Wang X, Chen Y, Yang Y. Characterization and comparison of microbiota in the gastrointestinal tracts of the goat (Capra hircus) during preweaning development. Front Microbiol 2019a;10:2125.
Li C, Wang W, Liu T, Zhang Q, Wang G, Li F, et al. Effect of early weaning on the intestinal microbiota and expression of genes related to barrier function in lambs. Front Microbiol 2018;9:1431.
Li F, Yang X, Cao Y, Li S, Yao J, Li Z, et al. Effects of dietary effective fiber to rumen degradable starch ratios on the risk of sub-acute ruminal acidosis and rumen content fatty acids composition in dairy goat. Anim Feed Sci Technol 2014;189:54–62.
Li G, Zhou S, Li C, Cai B, Yu H, Ma B, et al. Base pair editing in goat: nonsense codon introgression into FGF 5 results in longer hair. FEBS J 2019b;286:4675–92.
Lin L, Wang Y, Xu L, Liu J, Mao S. Microbiome–host co-oscillation patterns in remodeling of colonic homeostasis during adaptation to a high-grain diet in a sheep model. Animal Microbiome 2020;2.
Litvak Y, Byndloss MX, Tsolis RM, Bäumler AJ. Dysbiotic Proteobacteria expansion: a microbial signature of epithelial dysfunction. Curr Opin Microbiol 2017;39:1–6.
Liu G, Ding Y, Chen Y, Yang Y. Effect of energy intake and L-carnitine on fattening performance, carcass traits, meat quality, blood metabolites, and gene expression of lamb. Small Rumin Res 2022;183.
Liu H, Wang J, He T, Becker S, Zhang G, Li D, et al. Butyrate: a double-edged sword for health? Adv Nutr 2018;9:21–9.
Liu W, Mi S, Ruan Z, Li J, Shu X, Yao K, et al. Dietary tryptophan enhanced the expression of tight junction protein ZO-1 in intestine. J Food Sci 2017;82(2):562–7.
Lyte M, Villageliú DN, Crooker BA, Brown DR. Symposium review: microbial endocrinology—why the integration of microbes, epithelial cells, and neurochemical signals in the digestive tract matters to ruminant health. J Dairy Sci 2018;101:5619–28.
Marathe GK, Silva AR, Neto HCdCF, Tjoelker LW, Prescott SM, Zimmerman GA, et al. Lysophosphatidylcholine and lyso-PAF display PAF-like activity derived from contaminating phospholipids. J lipid Res 2001;42:1430–7.
Masoudi A, Raetz CR, Zhou P, Pemble IV, C W. Chasing acyl carrier protein through a catalytic cycle of lipid A production. Nature 2014;505:422–6.

McCoard SA, Cristobal-Carballo O, Knol FW, Heiser A, Khan MA, Hennes N, et al. Impact of early weaning on small intestine, metabolic, immune and endocrine system development, growth and body composition in artificially reared lambs. J Anim Sci 2020;98:skz356.
Medzhitov R, Janeway CA. Decoding the patterns of self and nonself by the innate immune system. Science 2002;296:298–300.
Moeser AJ, Pohl CS, Rajput M. Weaning stress and gastrointestinal barrier development: implications for lifelong gut health in pigs. Animal Nutrition 2017;3:313–21.
Munyaka PM, Rabbi MF, Khafipour E, Ghia JE. Acute dextran sulfate sodium (DSS)-induced colitis promotes gut microbial dysbiosis in mice. J Basic Microbiol 2016;56:986–98.
Potdar AA, Dube S, Naito T, Li K, Botwin G, Haritunians T, et al. Altered intestinal ACE2 levels are associated with inflammation, severe disease and response to anti-cytokine therapy in IBD. Gastroenterology 2020;160(3):809–22.
Ren W, Wang P, Yan J, Liu G, Zeng B, Hussain T, et al. Melatonin alleviates weanling stress in mice: involvement of intestinal microbiota. J Pineal Res 2018;64:e12448.
Rivera-Chávez F, Zhang LF, Faber F, Lopez CA, Byndloss MX, Olsan EE, et al. Depletion of butyrate-producing Clostridia from the gut microbiota drives an aerobic luminal expansion of Salmonella. Cell Host Microbe 2016;19:443–54.
Romaní-Pérez M, Agusti A, Sanz Y. Innovation in microbiome-based strategies for promoting metabolic health. Curr Opin Clin Nutr Metab Care 2017;20:484–91.
Sánchez E, De Palma G, Capilla A, Nova E, Pozo T, Castillejo G, et al. Colonization of infant's gut by Bacteroides is influenced by environmental and genetic factors linked to celiac disease risk. Appl Environ Microbiol 2011;77(15):1–27.
Schwab C, Berry D, Rauch I, Rennisch I, Ramesmayer J, Hainzl E, et al. Longitudinal study of murine microbiota activity and interactions with the host during acute inflammation and recovery. ISME J 2014;8:1101–14.
Song Y, Malmuthuge N, Steele MA, Guan LL. Shift of hindgut microbiota and microbial short chain fatty acids profiles in dairy calves from birth to pre-weaning. FEMS Microbiol Ecol 2017;94(3):fix179.
Takahara N, Kashiwagi A, Maegawa H, Shigeta Y. Lysophosphatidylcholine stimulates the expression and production of MCP-1 by human vascular endothelial cells. Metabolism 1996;45:559–64.
Toyonaga T, Araba KC, Kennedy MM, Keith BP, Wolber EA, Beasley C, et al. Increased colonic expression of ACE2 associates with poor prognosis in Crohn's disease. Sci Rep 2021;11(13533):1–15.
Trapnell C, Pachter L, Salzberg SL. TopHat: discovering splice junctions with RNA-Seq. Bioinformatics 2009;25:1105–11.
Wang C, Zhao J, Zhang H, Lee Y-K, Zhai Q, Chen W. Roles of intestinal bacteroides in human health and diseases. Crit Rev Food Sci Nutr 2020:1–19.
Wang S, Ma T, Zhao G, Zhang N, Tu Y, Li F, et al. Effect of age and weaning on growth performance, rumen fermentation, and serum parameters in lambs fed starter with limited Ewe–lamb interaction. Animals 2019;9:825.
Wang X, Niu Y, Zhou J, Zhu H, Ma B, Yu H, et al. CRISPR/Cas9-mediated MSTN disruption and heritable mutagenesis in goats causes increased body mass. Anim Genet 2018;49:43–51.
Yang J-Y, Kweon M-N. The gut microbiota: a key regulator of metabolic diseases. BMB reports 2016;49:536.
Yang J, Lee Y, Kim Y, Lee S, Ryu S, Fukuda S, et al. Gut commensal Bacteroides acidifaciens prevents obesity and improves insulin sensitivity in mice. Mucosal Immunol 2017;10:104–16.
Ye J, Coulouris G, Zaretskaya I, Cutcutache I, Rozen S, Madden TL. Primer-BLAST: a tool to design target-specific primers for polymerase chain reaction. BMC Bioinf 2012;13:1–11.
Ylä-Herttuala S, Palinski W, Rosenfeld M, Parthasarathy S, Carew T, Butler S, et al. Evidence for the presence of oxidatively modified low density lipoprotein in atherosclerotic lesions of rabbit and man. J Clin Invest 1989;84:1086–95.
Yu S, Zhang G, Liu Z, Wu P, Yu Z, Wang J. Repeated inoculation with fresh rumen fluid before or during weaning modulates the microbiota composition and co-occurrence of the rumen and colon of lambs. BMC Microbiol 2020;20:29.
Zhang K, He C, Xu Y, Zhang C, Li C, Jing X, et al. Taxonomic and functional adaption of the gastrointestinal microbiome of goats kept at high altitude (4800 m) under intensive or extensive rearing conditions. FEMS (Fed Eur Microbiol Soc) Microbiol Ecol 2021;97:fiab009.
Zhang K, Li B, Guo M, Liu G, Yang Y, Wang X, et al. Maturation of the goat rumen microbiota involves three stages of microbial colonization. Animals 2019;9:1028.
Zhang X, Choi FF, Zhou Y, Leung FP, Tan S, Lin S, et al. Metabolite profiling of plasma and urine from rats with TNBS-induced acute colitis using UPLC-ESI-QTOF-MS-based metabonomics–a pilot study. FEBS J 2012;279:2322–38.